Journal of Nuclear Materials 547 (2021) 152817

Contents lists available at ScienceDirect

Journal of Nuclear Materials

journal homepage: www.elsevier.com/locate/jnucmat

Quantifying the effect of hydride microstructure on zirconium alloys embrittlement using image analysis

Pierre-Clément A. Simon[a,*], Cailon Frank[a], Long-Qing Chen[b], Mark R. Daymond[d], Michael R. Tonks[c], Arthur T. Motta[a]

[a] Ken and Mary Alice Lindquist Department of Nuclear Engineering, PA, 16802, USA
[b] Department of Materials Science and Engineering, The Pennsylvania State University, University Park, PA, 16802, USA
[c] Department of Materials Science and Engineering, University of Florida, Gainesville, FL, 32611, USA
[d] Department of Mechanical and Materials Engineering, Queen's University, Kingston, Ontario, K7L 2N8, Canada

ARTICLE INFO

Article history:
Received 4 November 2020
Revised 9 January 2021
Accepted 12 January 2021
Available online 16 January 2021

Keywords:
Zirconium hydrides
Radial hydride fraction
Hydride continuity
Cladding embrittlement
Genetic algorithm

ABSTRACT

Because hydride microstructure can significantly influence Zr alloy nuclear fuel cladding's ductility, a new metric has been developed to quantify hydride microstructure in 2D micrographs and relate it to crack propagation. As cladding failure usually results from a hoop stress, this new metric, called the Radial Hydride Continuous Path (RHCP), is based on quantifying the continuity of brittle hydride particles along the radial direction of the cladding tube. Compared to previous metrics, this approach more closely relates to the propensity of a crack to propagate radially through the cladding tube thickness. The RHCP takes into account hydride length, orientation, and connectivity to choose the optimal path for crack propagation through the cladding thickness. The RHCP can therefore be more closely linked to hydride embrittlement of the Zr alloy material, thus creating a relationship between material structure, properties, and performance. The new definition, along with previously proposed metrics such as the Radial Hydride Fraction (RHF), the Hydride Continuity Coefficient (HCC), and the Radial Hydride Continuity Factor (RHCF), have been implemented and automated in MATLAB. These codes are made available with this publication as supplementary materials. These metrics were verified by comparing their predictions of hydride morphology against expected values in simple cases, and the implementation of the new metric was validated by comparing its predictions with manual measurements of hydride microstructure performed on ImageJ. The RHCP was also validated against experimental measurements of fracture behavior and it was shown to correlate with cladding failure better than previous metrics. The information provided by these metrics will help accurately assess cladding integrity during operation, transportation, and storage.

1. Introduction

Zirconium alloys are widely used in Light Water Reactors (LWRs) as fuel cladding material [1]. A fraction of the hydrogen produced by corrosion during normal operations is picked-up by the cladding. When the hydrogen concentration reaches the terminal solubility limit in the alloy, hydrogen precipitates into brittle hydrides platelets [1–5]. At the mesoscale, hydrides form platelets that are normally oriented along the tube circumferential direction but can be oriented radially under certain conditions [1,2,5]. Because cladding failure is usually caused by the presence of a hoop stress in the cladding, radial hydrides will fail early in the deformation process and ease crack propagation through the cladding thickness so that failure happens more easily. Thus, changes in hydride orientation can have a strong effect on cladding embrittlement [1,2,6–37]. Because of this, being able to quantify mesoscale hydride morphology from the point of view of its effect on ductility is of primary importance in assessing cladding integrity during normal operation, transportation, and dry storage [1].

Three main characteristics of hydride microstructure drive cladding failure under a hoop stress: first, the total hydrogen content and the fraction of the hydrogen that is precipitated into hydride platelets. Second, the fraction of radially oriented hydrides, and finally, how *continuous* hydrides are through the cladding thickness. Several microstructure metrics have been used to describe these characteristics of zirconium hydride morphology and their effect on crack initiation and propagation [1,2,10,15–17,38]. The first metric, the total hydrogen content, can be measured ex-

* Corresponding author.
E-mail address: pjs5523@psu.edu (P.-C. A. Simon).

https://doi.org/10.1016/j.jnucmat.2021.152817
0022-3115/

perimentally, and the hydride volume fraction can be estimated by metallography or x-ray diffraction [12–14,18–26]. While these two metrics do not specify the hydride distribution, other metrics relate more specifically to hydride morphology. Among them, the Radial Hydride Fraction (RHF) focuses only on the second characteristic [15], and other metrics such as the Hydride Continuity Coefficient (HCC) [8] and the Radial Hydride Continuity Factor (RHCF) [9] attempt to assess the third characteristic. In this work, we discuss these metrics used to quantify hydride morphology, review their shortcomings, and propose a new metric that more closely relates the hydride morphology to embrittlement. The approach presented in this paper is based on several assumptions. First, the hydrides are assumed to be significantly more brittle than the Zr matrix. This is mostly applicable to near room temperature testing. Second, the hydrides platelets are assumed to be infinitely long in the direction perpendicular to the plane of the micrographs. Lastly, hydride embrittlement is assumed to be caused by crack propagation through the thickness of a hydrided Zr component under a hoop stress.

1.1. Radial hydride fraction: a review

One of the more widely used metrics to quantify hydride morphology is the RHF. Defined between 0 and 1, the RHF corresponds to the resolved fraction of the total mesoscale hydride platelets that are oriented radially. The higher the RHF, the easier it can be for a crack to propagate radially through the cladding as a larger fraction of hydride platelets are oriented along its macroscale direction of propagation. The definition of the RHF can vary [1,2,6,7,10,13,15,27,29–37], but it is commonly defined using an expression similar to the one used by Colas in Ref. [2], where

$$RHF = \frac{\sum_i L_i f_i}{\sum_i L_i}, \tag{1}$$

where L_i is the length of the ith hydride particle, and f_i is the weight corresponding to the ith hydride. The sum is taken over all the hydrides. The weight of the hydrides is typically given by

$$f_i = \begin{cases} 0 & ; 0^\circ \leq \theta \leq 40^\circ \\ 0.5 & ; 40^\circ < \theta < 65^\circ \\ 1 & ; 65^\circ \leq \theta \leq 90^\circ \end{cases} \tag{2}$$

where θ is the angle (in degrees) of the hydride platelet habit plane relative to the circumferential direction. Thus, $\theta = 0^\circ$ and $\theta = 90^\circ$ correspond to a circumferential and a radial hydride, respectively.

One limitation of the RHF is that, since the metric does not differentiate between hydrides oriented within the ranges from 0° to 40°, 40° to 65°, and 65° to 90°, some microstructures with quite different hydride morphologies can end up having the same RHFs. Moreover, although the RHF accounts for hydride platelet orientation, it disregards hydride *connectivity*, i.e. how hydrides are arranged in a given microstructure. Fig. 1 shows two hypothetical cases, with the same RHF but where we can expect a far easier crack propagation on the left than on the right because of the different hydride separation in the two cases.

1.2. Hydride continuity: a review

As shown above, the resistance of the cladding to fracture is indeed not entirely determined by the RHF. It also depends on how close the hydride particles are to each other and how they align across the cladding thickness, along a likely path of crack propagation [1,8,9]. Hydride continuity has emerged as a metric to quantify how close hydrides are to each other in a particular microstructure and how they connect both ends of the cladding thickness [8,9]. High hydride continuity means that once a first hydride cracks at low strains, hydride particles create a continuous path through the cladding thickness, easing crack propagation.

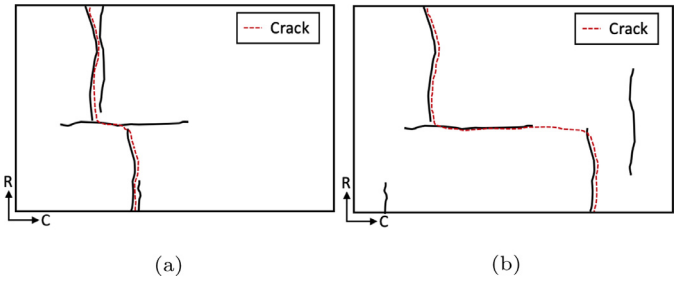

Fig. 1. Schematic drawing showing the effect of hydride continuity on crack propagation along the radial direction (R), where the hydrides are shown in black, and C describes the circumferential direction. Even though both configurations contain the same hydrides (only in different locations) and have the same RHF, configuration (a) has a higher hydride continuity than configuration (b). As such, a crack would propagate far more easily through micrograph (a) than (b). This example demonstrates the importance of accounting for hydride continuity when attempting to quantify hydride morphology.

Various metrics have been developed to define hydride continuity, including the HCC from Ref. [8] and the RHCF from Ref. [9]. In general, the values of these hydride continuity metrics vary between 0 and 1. Low values correspond to microstructures with few hydrides, and/or predominantly circumferential hydrides, and/or isolated hydrides. Conversely, high values correspond to a greater density of radial hydrides forming a path through the cladding thickness, which has negative consequences for the cladding embrittlement. An example of how the HCC is derived for a typical microstructure is illustrated in Fig. 2a [8,38]. The first step is to select a representative part of the microstructure. The HCC definition focuses on a rectangular band in the material, of height $L = 2.5$ mm along the radial direction and width $d = 0.11$ mm. The HCC is then given by

$$HCC = \frac{\sum_i HC_i}{L}, \tag{3}$$

where HC_i corresponds to the length of the ith radially projected hydride. Note that only the values of HC_i greater than 5 μm are included in the calculation for the HCC [8]. To make this measurement more representative of the microstructure, an average of different measurements of the HCC can be used. For example, in Ref. [38], the HCC is calculated as the average of three measurements performed at three different random places in a micrograph. The HCC is not as widely used as the RHF, but it has been used by several studies to quantify hydride morphology [26,38,39], and it has been slightly adapted to define it as a radial hydride length per unit area [23].

Fig. 2b provides a graphical illustration of the RHCF, a metric which was originally designed to predict the extent of a crack in a hydrided microstructure [9]. The RHCF is defined as the ratio

$$RHCF = \frac{\max(L_i)}{h_m}, \tag{4}$$

where h_m is the cladding wall thickness, and L_i is the length of the ith radially projected hydride within a 150 μm arc length, which roughly corresponds to distances covered by cracks during propagation [9].

These hydride microstructure continuity metrics attempt to quantify the link between hydride microstructure and crack propagation through the thickness of zirconium cladding. To properly do so, the definitions of the HCC or the RHCF should correspond to the mechanism of crack propagation. However, Fig. 3 shows that both the HCC and the RHCF metrics have limitations in relating the hydride microstructure to fracture behavior. The figure shows four schematic hydride configurations featuring different positions

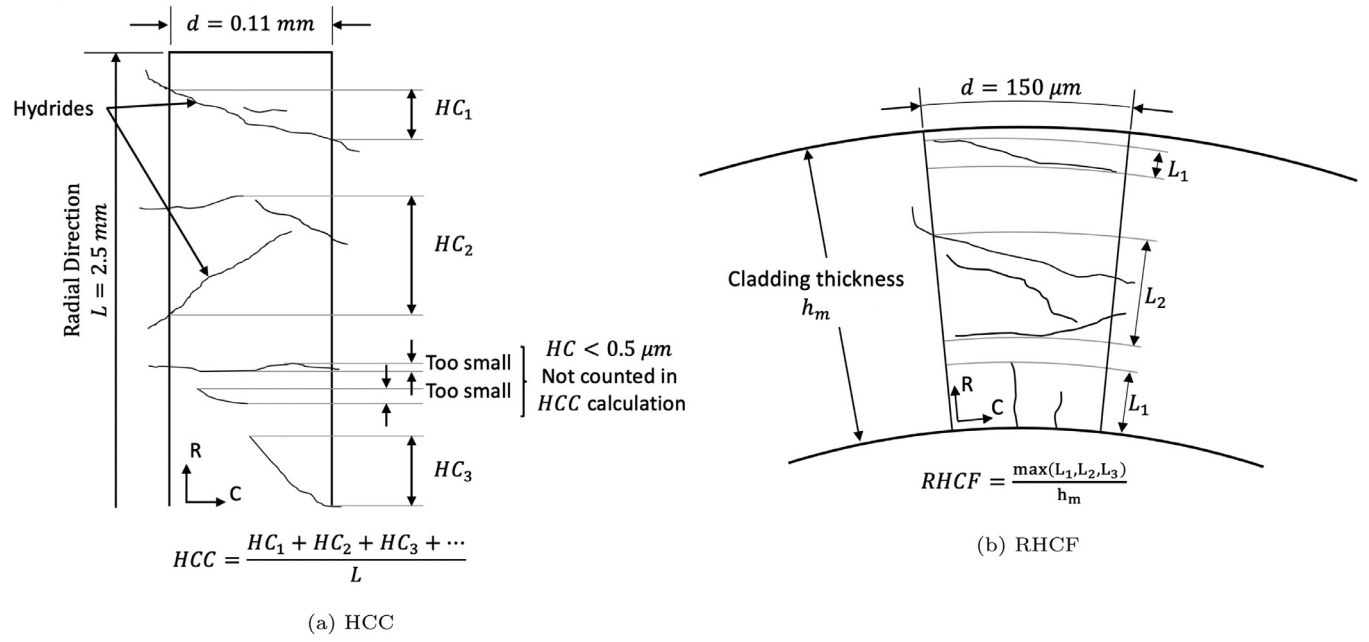

Fig. 2. Illustration of how the (a) Hydride Continuity Coefficient (HCC) [8,38] and (b) the Radial Hydride Continuity Factor (RHCF) [9] are defined for various microstructures. Both show the bands in which the RHCF and the HCC are derived, as well as how the projections are included in the calculations.

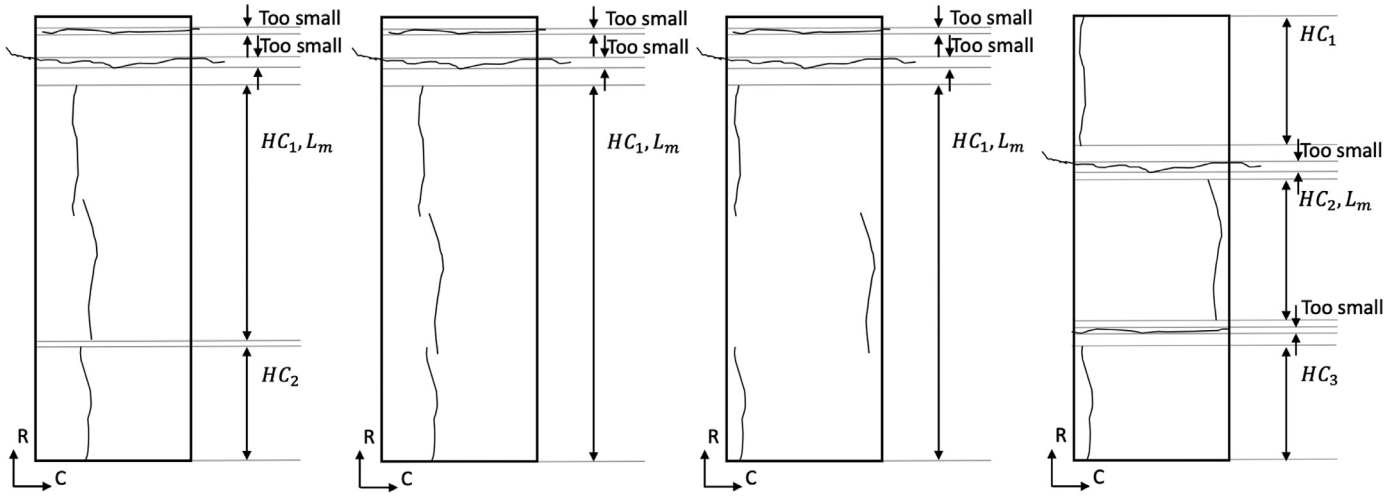

Fig. 3. Examples of model micrographs emphasizing the limitations of both the HCC and the RHCF. Each micrograph has the same RHF and the same hydrides, but they are positioned differently. (a) and (b) show that the RHCF can be sensitive to slight differences in vertical positioning of hydrides, while these variations would have little impact on crack propagation. (b) and (c) show that both the HCC and the RHCF are insensitive the hydride platelets being far apart within the band, even though this change in morphology would have a large impact on crack propagation. Finally, (c) and (d) show that not including the circumferential hydrides in the definition of the HCC and the RHCF prevents these definitions from considering cracks that propagate along circumferential hydrides to bridge between radial hydrides, thus providing misleading values of continuity.

for the same five hydrides which thus have the same RHF. Comparing these microstructures shows that micrographs with potentially similar cracking behavior can have significantly different RHCF values, and that micrographs with potentially different cracking behavior can have similar HCC or RHCF values. For example, the schematic hydride microstructures illustrated in Fig. 3a and b are very similar, as only a slight difference in the radial position of one of the hydrides differentiates them. These microstructures are thus expected to present similar cracking behaviors. However, while the HCC remains similar, the RHCF drastically changes between the two, suggesting that the microstructure in Fig. 3b is significantly more prone to crack propagation than that in Fig. 3a. This shows that the RHCF can be too sensitive to hydride configuration even when that difference is unlikely to affect the cracking path. Further the microstructures Fig. 3b and Fig. 3c have likely very different fracture behaviors, as hydrides are further apart in Fig. 3c than in Fig. 3b. However, both present the same HCC and RHCF values. Since both definitions are based only on the radial component of the hydride platelets, they are unable to distinguish between these two microstructures. Using only the radial component of the hydride platelets also leads both definitions to neglect the role of circumferential hydrides in crack propagation. In Fig. 3d, despite

having radial hydrides far apart from each other, crack propagation is expected to be easier than in Fig. 3c due to the presence of circumferential hydrides that can bridge the gap between radial hydrides. However, the HCC remains almost constant, while the RHCF decreases. This similarity inaccurately suggests that these two microstructures could present similar fracture behaviors or that the microstructure in Fig. 3c could actually be *more* prone to crack propagation than the one in Fig. 3d, which is not expected to be the case.

Both the RHF and the two hydride continuity metrics have been defined and used in the literature to quantify hydride microstructure and predict the fracture behavior of the material [1,2,8–10,15,16,38]. In this study, we develop an innovative approach for quantifying hydride continuity that more accurately predicts the material's fracture behavior. The new metric has been implemented in MATLAB and is verified and validated. In Section 2, we discuss the development of a new definition to characterize hydride continuity, called the Radial Hydride Continuous Path (RHCP). We describe the verification of the new definition in Section 3, and the validation of the genetic algorithm on which the definition is based in Section 4. The RHCP is then compared with existing metrics against experimental measurements in Section 5. In Section 6, we comment on the results and discuss the merits and shortcomings of this definition of hydride continuity. Finally, the results are summarized in Section 7. A link to the MATLAB codes developed during this project and the sets of microstructures used in the verification and validation processes are available in Section 8.

2. Hydride continuity: radial hydride continuous path

Given the previous metrics shortcomings, a good definition of the hydride continuity should link zirconium hydride microstructure and fracture behavior [8,9,38]. The goal of the definition introduced in this section is to quantify hydride microstructure in a way that relates directly to the mechanisms of crack propagation through the cladding thickness. This definition and its implementation in MATLAB are verified, validated, and compared to existing definitions.

2.1. New definition

The new definition introduced in this study is guided by the principle that the crack propagates through the path of least resistance. As shown in Refs. [20,40,41], when a crack propagates in a hydrided sample, cracks nucleate in neighboring hydrides, before connecting to the main crack. The crack thus primarily propagates from one hydride to the next following the path of least resistance. If each possible path through the cladding thickness were evaluated, the path of least resistance would provide an evaluation of hydride continuity in the sample. Following this approach, this study provides a new definition of the hydride continuity, called the Radial Hydride Continuous Path, defined as

$$RHCP = \max_x \left(RHCP_x\right), \tag{5}$$

where RHCP_x is the evaluation of a given path x across the microstructure. RHCP_x is further defined as

$$RHCP_x = \frac{(L - x_{Zr})w_{Zr} - x_{ZrH}w_{ZrH}}{L(w_{Zr} - w_{ZrH})}, \tag{6}$$

where L is the height of the domain, potentially equal to the cladding thickness, x_{Zr} and x_{ZrH} are the distances traveled in the zirconium and hydride phase, respectively, and w_{Zr} and w_{ZrH} are the penalties associated with the zirconium and hydride phase, respectively. The penalties w_{Zr} and w_{ZrH} represent how much resistance a path encounters when traveling in the zirconium and hydride phases. To ensure that this definition relates to crack propagation, the penalties are defined as the fracture toughnesses of the two phases at room temperature, namely $w_{Zr} = 50\ \mathrm{MPa}\sqrt{m}$ and $w_{ZrH} = 1\ \mathrm{MPa}\sqrt{m}$ [42–44] for this study. The reported fracture toughness of the zirconium material depends on the geometry of the sample and the conditions of the test. While values between 38 $\mathrm{MPa}\sqrt{m}$ and 77 $\mathrm{MPa}\sqrt{m}$ have been reported for plane strain specimen (thick plates) [42,43], values around 96 $\mathrm{MPa}\sqrt{m}$ have been reported for cladding geometry [38,43,45]. However, because the cladding geometry does not satisfy ASTM-E813 requirements for fracture testing, this study used a value of 50 $\mathrm{MPa}\sqrt{m}$, which falls within the range measured in [42,43]. It is important to note that the fracture toughness values of the zirconium provided in Refs. [42,43,45] were measured in polycrystal materials, which corresponds to the current study, and not in single grain zirconium samples. Moreover, although the hydride contribution to crack propagation is well established, it remains unclear how the crack propagates through hydrides, i.e. whether the hydride itself or the hydride/matrix interface cracks. In any case, the uncertainty about the appropriate values to use for the hydride phase and the zirconium phase is acceptable. As the ratio w_{Zr}/w_{Zr} remains large, hydrides drive crack propagation. Predictions of the algorithm are not expected to change significantly by reducing w_{ZrH} or increasing w_{Zr} as long as the ratio of the two remains of this order of magnitude.

A variation of this metric is also introduced to allow for ductile crack propagation. Since in regions with low hydride concentration, cracks often propagate at 45° angles rather than in straight lines in ductile materials like Zr (maximum stress direction), an additional penalty is introduced to favor an orientation of the path in the zirconium phase at 45°. This orientation-dependent variation is defined as

$$RHCP^{\theta_0} = \max_x \left(RHCP_x^{\theta_0}\right), \tag{7}$$

where θ_0 is the desired angle with respect to the radial direction for the path in the matrix phase, $\theta_0 = 45°$ for ductile metals like zirconium, and $\mathrm{RHCP}_x^{\theta_0}$ is the evaluation of a given path x. The $\mathrm{RHCP}_x^{\theta_0}$ is defined as

$$RHCP_x^{\theta_0} = \frac{\left(\frac{L}{\cos(\theta_0)} - \sum_i x_{Zr,i}\left(1 + Wg^{\theta_0}(\theta_i)\right)\right)w_{Zr} - x_{ZrH}w_{ZrH}}{L\left(\frac{w_{Zr}}{\cos(\theta_0)} - w_{ZrH}\right)}, \tag{8}$$

where $x_{ZrH,i}$ is the length of straight sections of the path in the zirconium phase with an orientation with respect to the radial direction equal to θ_i. Here also,

$$g^{\theta_0}(\theta) = (\theta_0 + \theta)^2(\theta_0 - \theta)^2, \tag{9}$$

is a double-well function centered around $\pm\theta_0$, and W a penalty defining the additional weight given to a path in zirconium when its orientation differs from θ_0. For high values of W, orientation different from θ_0 are heavily penalized, and the crack paths predicted by the algorithm will closely respect the orientation defined by θ_0. However, having a very large W can hinder the convergence of the genetic algorithm. In this work, $W = 13$ was found to be a good compromise and used throughout the study.

These definitions define the new metric of hydride continuity, the RHCP, between 0 and 1, with 0 indicating a total absence of hydrides (i.e. crack growth through an unhydrided material), and 1 corresponding to hydride precipitates being continuous through the cladding thickness. However, these definitions are only useful when coupled with an algorithm that can evaluate and find paths across the cladding thickness, evaluate them, and find the path x that maximizes RHCP_x or $\mathrm{RHCP}_x^{\theta_0}$ to provide the RHCP or the RHCP^{θ_0}.

2.2. A genetic algorithm to find the best path

A genetic algorithm was implemented to find the path of least resistance, i.e. the path x that maximizes $RHCP_x$. This algorithm is adapted from recent work by Hilty et al. on thermal resistance [46]. Given a set of initial paths, called the population, the genetic algorithm randomly selects two paths, called parents, and combines them to creates a third path, called the child. The child is then improved by smoothing it and its $RHCP_x$ value is determined. If its $RHCP_x$ value is higher than the $RHCP_x$ value of one of its parents, the child then replaces its worst parent in the population. By doing so over several generations, the genetic algorithm converges towards a path that maximizes the $RHCP_x$ values of its population, thus providing a good estimate of the RHCP of the microstructure. The MATLAB code is available in Section 8, along with detailed information about the algorithm. It is important to note that genetic algorithms are not guaranteed to provide the global optimum solution and sometimes only provide a local optimum solution. This can be an issue when there are many hydrides in a single micrograph. Dividing the micrographs into vertical bands, finding their local maxima, and then merging the paths from different bands together to find a global maximum can improve predictions. The genetic algorithm and the definitions of the RHCP and the $RHCP^{45}$ are verified and validated in the following sections.

It can be noted that no assumption is made about the origin of the crack path. The position of the crack path at the top and bottom of a given microstructure is a result of the genetic algorithm's search for the best path. It is based in the hydride microstructure alone, and not the result of the researchers' decision.

3. Verification of the MATLAB implementation

3.1. Verification on simple microstructures

The MATLAB implementations of the RHCP and the $RHCP^{45}$ metrics, quickly presented in Appendix A, have been verified on schematic micrographs with known expected values. The HCC and the RHCF definitions were also implemented in MATLAB and used on the schematic micrographs as a reference. The MATLAB implementations of the four metrics are available in Section 8. The microstructures shown in Figs. 4 and 5 test the definitions and the algorithms for several schematic hydride configurations. For each configuration, we provide the measured and expected values for all

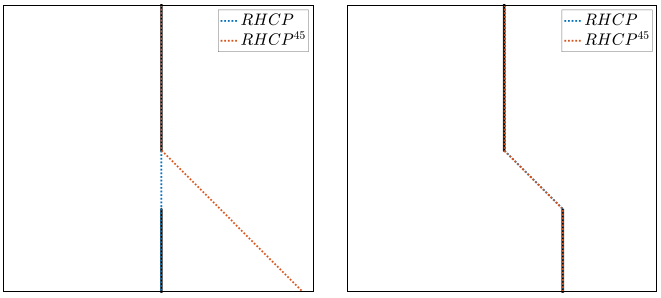

(a)
$RHF = 1$
$HCC = 0.798\ vs\ 0.800$
$RHCF = 0.508\ vs\ 0.500$
$RHCP = 0.800\ vs\ 0.800$
$RHCP^{45} = 0.504\ vs\ 0.500$

(b)
$RHF = 1$
$HCC = 0.797\ vs\ 0.800$
$RHCF = 0.508\ vs\ 0.500$
$RHCP = 0.715\ vs\ 0.715$
$RHCP^{45} = 0.791\ vs\ 0.800$

Fig. 5. Verification schematic micrographs, corresponding RHF values, and results for the HCC, RHCF, RHCP, and $RHCP^{45}$ metrics. Hydrides are shown in black, and the paths found by the RHCP and the $RHCP^{45}$ are shown in blue and red, respectively. The caption of each image provides the RHF and, for each continuity metric, the value determined by the MATLAB implementations versus the expected value. This fourth set is designed to expose the difference between the RHCP and the $RHCP^{45}$. In (a), the hydrides are aligned radially, which leads to a high RHCP but a low $RHCP^{45}$ since the gap between the hydrides cannot be linked by a 45 degree path. In (b), the hydrides are directly linked by a 45 degree angle path, which is found by both definitions. In this case, the RHCP is slightly lower than in (a), but the $RHCP^{45}$ increases from 0.5 in (a) to 0.8 in (b). This comparison shows that the $RHCP^{45}$ is more configuration-dependent that the RHCP. As a result, determining which one of the two configurations is more continuous depends on the definition being used. (For interpretation of the references to color in this figure legend, the reader is referred to the web version of this article.)

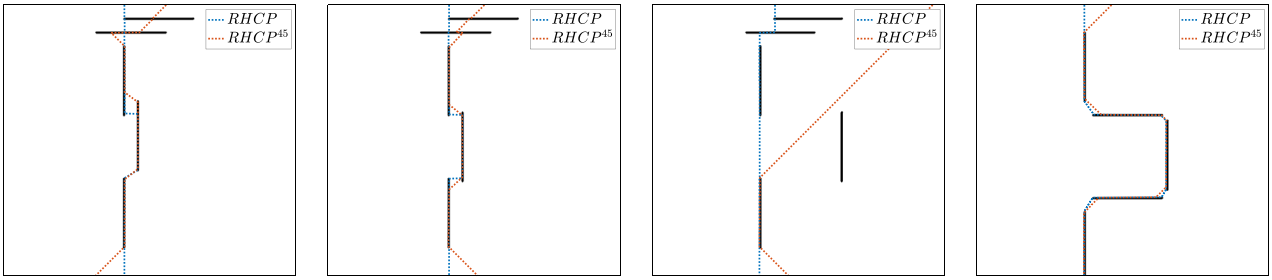

(a)
$RHF = 0.600$
$HCC = 0.711\ vs\ 0.700$
$RHCF = 0.457\ vs\ 0.450$
$RHCP = 0.643\ vs\ 0.640$
$RHCP^{45} = 0.634\ vs\ 0.625$

(b)
$RHF = 0.600$
$HCC = 0.741\ vs\ 0.740$
$RHCF = 0.741\ vs\ 0.740$
$RHCP = 0.652\ vs\ 0.648$
$RHCP^{45} = 0.623\ vs\ 0.623$

(c)
$RHF = 0.600$
$HCC = 0.742\ vs\ 0.740$
$RHCF = 0.742\ vs\ 0.740$
$RHCP = 0.519\ vs\ 0.520$
$RHCP^{45} = 0.138\ vs\ 0.180$

(d)
$RHF = 0.600$
$HCC = 0.746\ vs\ 0.750$
$RHCF = 0.255\ vs\ 0.250$
$RHCP = 0.704\ vs\ 0.708$
$RHCP^{45} = 0.659\ vs\ 0.744$

Fig. 4. Verification schematic micrographs, corresponding RHF values, and results for the HCC, RHCF, RHCP, and $RHCP^{45}$ metrics. Hydrides are shown in black, and the paths found by the RHCP and the $RHCP^{45}$ are shown in blue and red, respectively. The caption of each image provides the RHF and, for each continuity metric, the value determined by the MATLAB implementations versus the expected value. This set contains micrographs similar to the ones presented in Fig. 3. They all contain the same three radial hydrides and two circumferential hydrides, so the RHF is the same for all schematic micrograph. The results show that the genetic algorithm is able to handle microstructures with several hydrides and find the best path. Moreover, the shortcomings already described in Fig. 3 for the HCC and the RHCF are overcome by the RHCP and the $RHCP^{45}$, which provide a more robust quantification of the hydride microstructure. However, it is important to note that the RHCP and the $RHCP^{45}$ provide significantly different measures for (c), which is discussed later. (For interpretation of the references to color in this figure legend, the reader is referred to the web version of this article.)

four definitions. We also show the paths that were provided by the genetic algorithm for both the RHCP and the RHCP^{45} definitions.

The schematic micrographs shown in Fig. 4 are similar to the ones shown in Fig. 3 to emphasize some of the limitations of the RHF, the HCC, and the RHCF definitions and show that the new metrics developed in this study, the RHCP and the RHCP^{45}, overcome these limitations and thus more accurately quantify hydride continuity. The measurements are accurate for all definitions, as MATLAB predictions shown in Fig. 4 are very close to the expected values. This shows that the algorithm works and that the definitions were properly implemented in MATLAB. The hydrides were found by the genetic algorithm, and the paths use them to maximize the RHCP while connecting both ends of the microstructure. The genetic algorithm can handle microstructures with several hydrides and find a very good approximation of the expected best path. As expected, the path found for the RHCP definition minimizes the length of the path through the zirconium phase, while the path found for the RHCP^{45} definition traverses the zirconium at an angle of $\theta_0 = 45^\circ$ to minimize the penalty. Contrarily to previous metrics, the new metrics are able to determine that Fig. 4a and b are similar, but that Fig. 4c is less continuous than either Fig. 4a or Fig. 4b due to the circumferential separation between hydrides. Moreover, the RHCP and the RHCP^{45} are also able to quantify the role of circumferential hydrides in bridging radial hydrides, which was overlooked by previous metrics. As a result, we can expect that the new metrics proposed in this study provide a more robust quantification of the hydride microstructure then previous metrics.

However, it is important to note that even if the new metrics often give somewhat similar values to quantify hydride continuity (see Fig. 4), this is not always the case. For example, the microstructure given in Fig. 4c provides RHCP = 0.520 and RHCP^{45} = 0.180. This is because the RHCP^{45}, due to its additional angle constraint, is more sensitive to changes in hydride configurations. Fig. 5b provides two similar microstructures to emphasize this point. The only difference between the microstructures is in the horizontal position of the short hydride at the bottom of the microstructures. When the hydrides are aligned in Fig. 5a, RHCP^{45} finds it more favorable to ignore this hydride and form a 45° angled path in the zirconium matrix. It is only when the short hydride is oriented in a way that allows for a 45° angled bridge between the two hydrides that the RHCP^{45} definition uses this hydride to go through the microstructure. The RHCP^{45} value thus varies greatly depending on the hydride configuration, while the predictions from the RHCP are more stable. The RHCP^{45} quantifies Fig. 5b as more continuous than Fig. 5a, whereas the RHCP draws the opposite conclusion.

3.2. Verification on real microstructures

Now that the genetic algorithm and the new metrics for hydride continuity have been verified on schematic micrographs, it is important to see how the algorithm performs on real zirconium hydride microstructures. Real microstructures require binarization before analysis. Binarization identifies the pixels of the image as either part of the hydride phase, or part of the zirconium matrix. During that process, some of the imperfections present on the micrographs, i.e. dust, scratches, other particles can be filtered out of the microstructure. Fig. 6 shows how an original micrograph can be binarized by the MATLAB code developed in this study. More information is available in Section 8.

Unlike the verification micrographs used in Section 3.1, metallographs from real microstructures exhibit a degree of complexity that could make it challenging for the genetic algorithm to find the best path. The effectiveness of the band feature introduced in Section 2.2 to solve this issue is tested on the real microstructure shown in Fig. 6. Fig. 6 presents the original micrograph, its binarized version, as well as the best path found using the whole image at once, and the best path found when dividing the image into vertical bands before merging the paths from each band to find a better path.

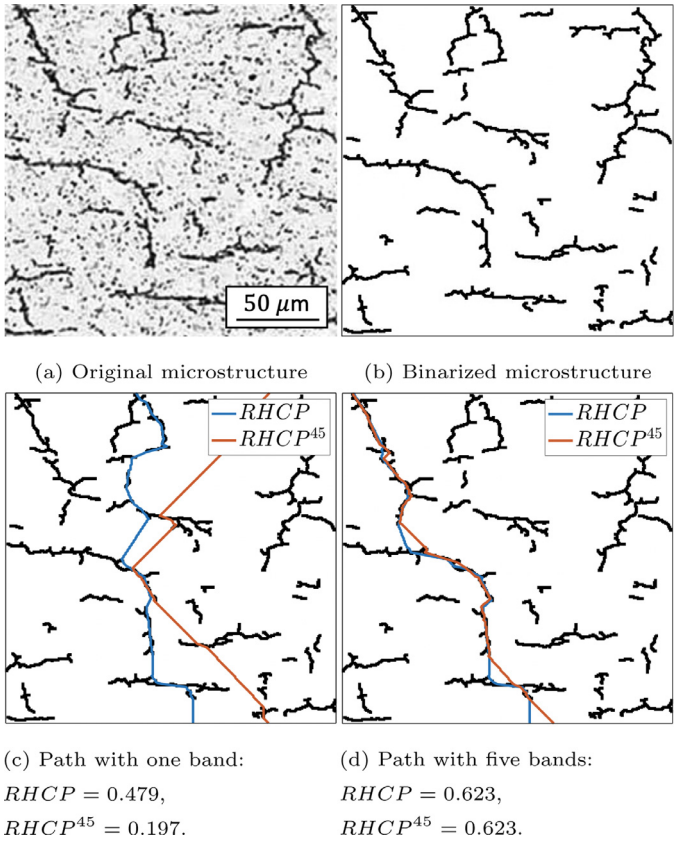

(a) Original microstructure (b) Binarized microstructure

(c) Path with one band: $RHCP = 0.479$, $RHCP^{45} = 0.197$.

(d) Path with five bands: $RHCP = 0.623$, $RHCP^{45} = 0.623$.

Fig. 6. Hydride microstructure from Ref. [47] (a), binarized version of the microstructure (b), and the paths found by the genetic algorithm while using one (c) and five (d) bands. The increases from $RHCP = 0.479$ to $RHCP = 0.623$ and from $RHCP^{45} = 0.197$ to $RHCP^{45} = 0.623$ show that using several bands is an effective way of improving the predictions of the genetic algorithm. The micrograph size is 200 μm × 200 μm.

It appears that dividing the images into bands before merging them again allows the algorithm to find a higher RHCP or RHCP^{45} value by avoiding local maxima. Without using the band feature, the RHCP of the microstructure is evaluated at 0.515, whereas while using five bands, the algorithm finds a path corresponding to RHCP = 0.653. Similarly, the RHCP^{45} of the microstructure is underestimated at 0.197 with one band, but a measurement with five bands provides RHCP^{45} = 0.653. Thus, the band feature allows the genetic algorithm to analyze complex microstructures and consistently evaluate their RHCP or RHCP^{45} values. Selecting the most appropriate number of bands is a balance between the desired accuracy and computational cost, and might depend on the hydride content and orientation. In this study, however, we have found that using a band width of 40 μm provided accurate results. Using more than 5 bands in a 200 μm large micrograph did not provide significantly better results, independently of hydride content, shape, and orientation.

To summarize, the genetic algorithm and the two metrics introduced in this study have been successfully verified. These metrics overcome some of the limitations of previously existing metrics and offer a robust way to relate complex hydride microstructures to fracture behavior. Two aspects of the RHCP and the RHCP$^{\theta_0}$ implementations require validation. First, we show that the genetic algorithm is able to find a good approximation of the best paths,

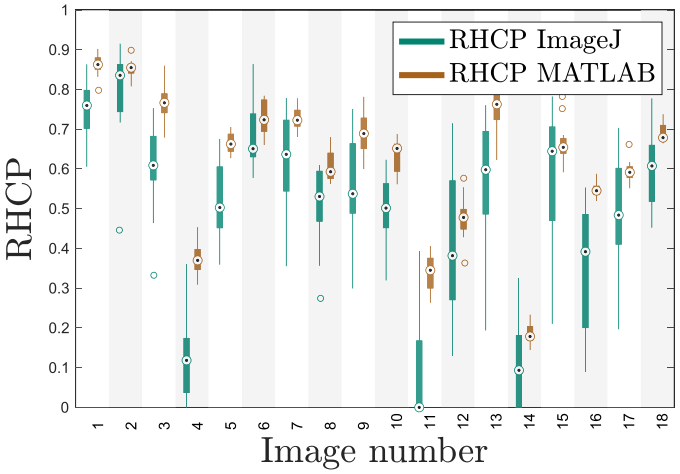

Fig. 7. Results of the validation of the new RHCP implementation. For each micrograph, this graph shows the results for both the ImageJ measurements and the MATLAB results. For each, it shows the value of the median with a black dot, the 25th and 75th percentiles with the bottom and top edges of the box, and the extremes with the whiskers. Outliers are plotted using a circle. The RHCP predictions made with the MATLAB code are, in general, higher than manual measurements, which indicates that the MATLAB code is better than humans at finding the best path. Measurements made using the MATLAB code are also consistent across users, whereas manual measurements tend to vary depending on the user.

even outperforming manual measurements. Second, we prove that the RHCP and the RHCP^{45} definitions correlate to fracture behavior.

4. Validation of the genetic algorithm

The genetic algorithm used to derive the best paths for the RHCP and the RHCP$^{\phi_0}$ is validated by comparing its prediction on real hydride microstructures against predictions made by researchers. Micrographs were found in Ref. [2,47–49] and are listed in Section 8. Twelve volunteers were given the validation microstructures provided in Section 8 and were asked to obtain the RHCP of these microstructures by using the MATLAB algorithm produced in this study. They were also asked to use the binarized images created by the MATLAB code and plot the best path across the microstructure manually in ImageJ. This procedure tests the ability of the genetic algorithm to find the best path in complex microstructures. A link to the microstructures and the detailed instructions given to volunteers are available in Section 8. Predictions were then compared in Fig. 7 and analyzed.

Comparing the RHCP values of the MATLAB code and the manual measurements in Fig. 7 shows that the MATLAB prediction is, in general, higher than manual measurements, which means that it is better able to find the best path in a microstructure. The median of the RHCP measurements made using MATLAB is, on average, 0.125 higher than the median of the manually obtained measurements, with a significant maximum difference of 0.35 for micrograph 11. Another advantage of the MATLAB code is that it reduces the influence of the user on the measured RHCP value. In this case, both methods, MATLAB and ImageJ, depend on the user during the binarization process. In addition to this dependence, the predictions of the MATLAB code only depend on random variations in the genetic algorithm, which are reasonably small. In contrast, manual measurements performed using ImageJ depend on the ability of the user to predict the best crack path through the microstructure. These differences make the MATLAB measurements significantly more consistent with around 3 times less variation, as the difference between the 25th and 75th percentiles is, on average, equal to 0.050 when using the MATLAB algorithm, compared to 0.170 for the manual measurements.

Moreover, using the MATLAB code rather than performing measurements manually saves a significant amount of user time. Guessing the path manually on ImageJ requires the user to take the time to manually draw the path on the microstructure. When using the MATLAB code, the user only needs to binarize the microstructures using the GUI, and then let the code analyze the microstructures. Manual measurements on the validation microstructures took about 56 min on average, whereas using the MATLAB code took about 16 min on average.

Since the genetic algorithm is the same for both RHCP and RHCP^{45}, the results presented above are expected to be valid for the RHCP^{45} MATLAB implementation. The genetic algorithm is expected to perform even better against humans in this case, as the constraint on the path orientation makes paths harder to optimise manually.

5. Validation of the RHCP and the RHCP^{45} metrics against experiments

Now that the definition and implementation have been verified, and the genetic algorithm has been validated against humans, we show that the RHCP metric can quantify hydride microstructure in a way that correlates with the fracture behavior of the materials. To that end, we used the microstructures and the experimental results from Ref. [50], in which ring compression tests were carried out on pre-hydrided zircaloy samples to measure the material toughness as a function of hydride microstructure. In total, six different types of results were used: samples with circumferential hydrides and low hydrogen content (150–210 wt.ppm), samples with circumferential hydrides and high hydrogen content (550-1050 wt.ppm), and samples with radial hydrides and low hydrogen content (100–150 wt.ppm), all at 25 °C and at 150 °C. The microstructures from Figs. 7 and 9 in Ref. [50] were each analyzed using the MATLAB codes to determine its RHF, HCC, RHCF, RHCP, and RHCP^{45} values and the most likely crack path according to the RHCP and the RHCP^{45} metrics. The toughness data for low-temperature samples provided in Fig. 11 in Ref. [50] was then extracted, and it was plotted as a function of the hydrogen content, which was provided by the study, the RHF, the HCC, the RHCF, the RHCP, and the RHCP^{45}. For each, a linear regression was performed for 25 °C samples and for both 25 °C and 150 °C samples. The quality of these linear fits attests to how well each metric correlates with the material fracture behavior. The results are shown in Fig. 8.

Fig. 8a shows that hydrogen content does not correlate well with fracture behavior, as expected. Specifically, the hydrogen content does not differentiate between samples with radial hydrides, which can become brittle with only a hundred wt.ppm, and samples with circumferential hydrides. The RHF quantifies hydride orientation and thus performs better than hydrogen content in predicting the fracture behavior as shown in Fig. 8b. The RHF, however, does not differentiate between circumferential samples with low and high amounts of hydrogen. Two sets of samples at 25 °C have similar RHF values (0.15 and 0.23), but exhibit significantly different values for the fracture energy/area (557 KJ/m^2 and 81 KJ/m^2) due to their different hydrogen content (176 wt.ppm and 562 wt.ppm [50]). The fact that circumferential hydrides can have a negative impact on cladding integrity has been experimentally observed in Ref. [22], but is not accounted for by the RHF; adding circumferential hydrides to a radial microstructure only decreases the RHF.

Because they quantify the hydride arrangement and continuity in addition to hydride orientation, the HCC, the RHCF, the RHCP, and the RHCP^{45} correlate better with fracture behavior than the RHF. Given the quality and the linear fit and the stability of the fit between 25 °C and both 25 °C and 150 °C, these four metrics

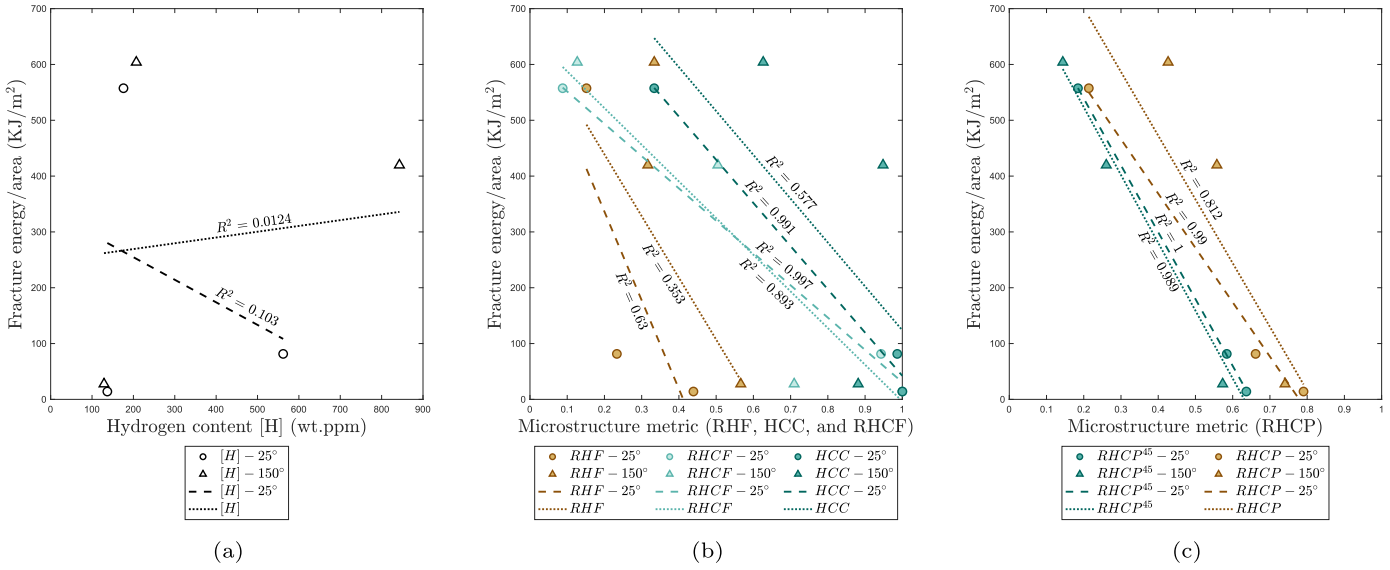

Fig. 8. Correlations between different hydride microstructure metrics and the fracture energy/area (KJ/m^2) provided in Ref. [50] for different temperatures (25 °C and 150 °C). The lines show the linear interpolations using the data from 25 °C only, and from all the data, along with the r-square value of these fits. (a) shows that the hydrogen content does not correlate well with fracture behavior as it does not differentiate between radial and circumferential hydrides. (b) and (c) show that the RHF, the RHCF, the HCC, the RHCP, and the RHCP^{45} all correlates with fracture behavior, especially for room temperature tests. RHCP^{45} performs better than the other metrics, giving higher r-square values and consistent fits.

can be ranked as follows: the HCC, with lesser performances, the RHCP, the RHCF, and then the RHCP^{45}, with better performances than any other metrics introduced in this study. The HCC seems to overestimate the continuity of circumferential hydrides, especially at higher hydrogen content, since these circumferential hydrides are rarely perfectly flat and disconnected. Despite the shortcomings discussed in Sections 1 and 3, the RHCF performs surprisingly well on these microstructures. It differentiates most microstructures, even if it does underestimate the hydride continuity in the sample with circumferential hydride and high hydrogen content. The RHCF was designed to perform well for fractures occurring in homogeneous hydride microstructures in ring compression tests, which corresponds to the experimental results used here [50]. It is, however, expected to be less accurate for samples with heterogeneous hydride content (i.e. with a blister or a rim). Moreover, it is important to note that both the HCC and the RHCF quickly yield values close to 1 for samples with radial hydrides, which might prevent them from differentiating between such samples.

The RHCP performs well for radial hydrides and circumferential hydrides with high hydrogen content, but varies more when quantifying samples with circumferential hydrides and low hydrogen content, which relates to the shape of the crack path it uses and is discussed later. The RHCP^{45}, however, quantifies all the microstructures appropriately and correlates remarkably well with fracture behavior. In addition to high-quality linear fits, both fits (using values from tests conducted at 25° and 25 °C plus 150 °C) are very similar, which attests to its stability.

As shown in Fig. 8c, the RHCP^{45} seems to perform better than the RHCP, since the linear regressions are a better fit for the RHCP^{45} than for the RHCP. The prediction differences between the RHCP and the RHCP^{45} were discussed in Section 3, where it was noted that the RHCP is more stable with respect to microstructure changes, while the RHCP^{45} better describes the crack propagation mechanisms of ductile materials. At low-temperatures, the zirconium matrix is ductile and tends to crack at a 45° angle to the applied stress. In these conditions, the RHCP^{45} describes the crack path more accurately than the RHCP and thus correlates better with fracture behavior. Fig. 9 shows one circumferential and one radial microstructure cracked at room temperature provided

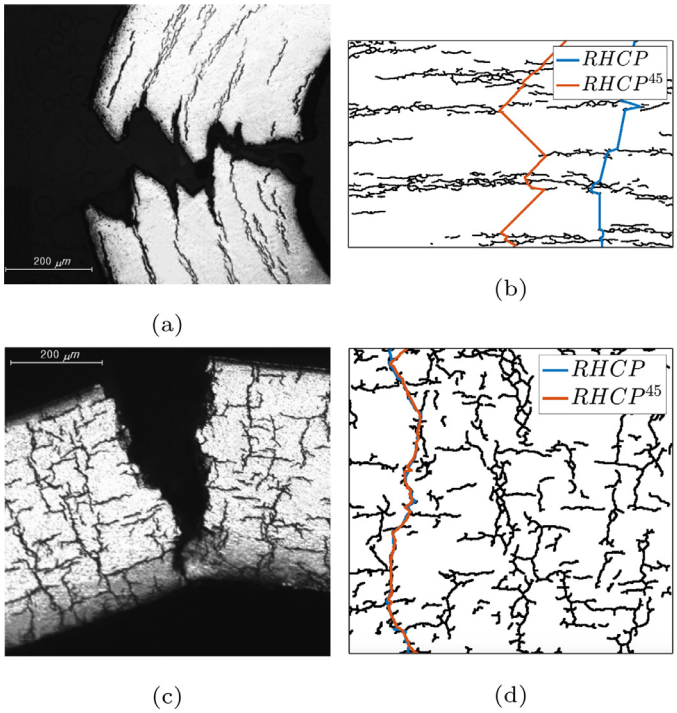

Fig. 9. Comparison of the path found by the RHCP and the RHCP^{45} metrics against experimental crack paths in microstructures with circumferential and radial hydrides. (a) and (c) show cracked microstructures from Ref. [50] with circumferential and radial hydrides, respectively, and (b) and (d) show the paths predicted by both the RHCP and the RHCP^{45} metrics on uncracked micrographs of the same samples. The RHCP^{45} describes the crack path more accurately than the RHCP, especially for circumferential hydrides, and thus correlates better with fracture behavior.

in Figs. 7 and 9 in Ref. [50], along with the crack paths predicted by the RHCP and the RHCP^{45} on uncracked microstructures from the same study. The crack observed in the microstructure with circumferential hydrides in Fig. 9a propagates along a 45° angle from hydride to hydride, which is reflected in the RHCP^{45} path shown in

Fig. 9b. The RHCP path, however, minimizes the distance traveled in the zirconium phase and links hydrides almost radially, leading to poorer predictive performance for samples with low hydrogen content and a larger fraction of circumferential hydrides. The crack observed in the microstructure with radial hydrides presented in Fig. 9c propagated radially through the cladding thickness, since hydrides created a continuous path. Both the RHCP and the RHCP^{45} were able to find similar radial paths through the microstructure using radial hydrides. The predicted crack path closely resembles the experimentally observed crack shape.

It is important to note that for this study, only the samples cracked at room temperature and at 150 °C were used. At higher temperatures, hydrided zirconium transitions from relatively brittle to relatively ductile, and the fracture mechanisms can change [9,12,25,26,41,51]. Moreover, since hydrides dissolve at high temperatures, the high-temperature microstructures are different from those observed at low temperatures. Both of these effects lead to a diminishing influence of the hydride microstructure on embrittlement at higher temperatures, as has been experimentally observed in Ref. [22,44]. The RHCP and the RHCP^{45} can account for the changing properties of the phases by adapting the fracture toughness coefficients used in the definition of RHCP provided in Eq. (6), but the RHCP^{45}'s performance is expected to decline as cracks propagate radially rather than at a 45° angle [41]. Even with RHCP, however, using a low-temperature microstructure to predict high-temperature cracking is expected to affect the reliability of the results and we advise using high-temperature micrographs when possible.

6. Discussion

This study aims to improve hydride microstructure quantification to relate it to embrittlement and provide new tools for researchers to easily and reliably quantify their microstructures. To that end, two new metrics, the RHCP and the RHCP^{45}, have been developed, and their MATLAB implementations are available in Section 8. Whereas previous metrics focused on hydride morphology alone, the new metrics are based on mechanisms of crack propagation and thus correlate better with hydride embrittlement. It is challenging to provide a definition that remains stable with respect to hydride configuration while being representative of crack propagation mechanisms, and each metric focuses on one aspect of this challenge. The RHCP provides no constraints on the crack direction within the zirconium matrix, while the RHCP^{45} orients the crack path with a 45° angle in the matrix. The RHCP and the RHCP^{45} have been shown to provide accurate and reliable quantification of the hydride microstructure. The RHCP^{45}, in particular, outperformed existing metrics. As shown in Section 3, in contrast to other metrics, the RHCP metrics account for the role of circumferential hydrides in promoting hydride embrittlement. They also recognize differences in microstructures that are overlooked by other metrics. The RHCP and the RHCP^{45} have been validated against experimental measurements of fracture behavior in Section 5 and have shown to correlate closely to embrittlement.

It is important to note that the new metrics introduced in this study do not make any assumptions on the crack propagation direction in the microstructure (i.e. top to bottom versus bottom to top). As such, it makes only limited assumptions on the loading conditions, i.e., that the load is applied in the circumferential direction, which corresponds to a hoop stress for cladding material. Although the algorithm was tested in the case of ring test compression tests, it is expected to perform just as well for failure of cladding material due to internal pressure, or failure of sheet material. However, more work is still needed to verify how well the new metric correlates with fracture behavior for different loading conditions.

Moreover, the MATLAB implementations of the RHF, the HCC, the RHCF, the RHCP, and the RHCP^{45} offer the advantages of automated analysis over manual measurements. Predictions are less dependent on the user's subjective decisions, hence providing more robust, reproducible measurements. It is also more accurate, in particular for the RHCP and the RHCP^{45}, and requires less time than manual measurements.

Despite significant improvements that this study offers, the RHCP and the RHCP^{45} metrics have limitations. Even though RHCP and RHCP^{45} have been shown to be more stable than previous metrics, it is important to select a representative section of the sample to quantify hydride microstructure. In a given sample, the hydride microstructure can change drastically and different RHF, RHCF, HCC, RHCP, and RHCP^{45} values can be obtained depending on the location in the sample. It is preferable to quantify the microstructure at a few different locations in the sample to obtain more globally representative results. When possible, the microstructure should be quantified in the location where cracks are most likely to form. This corresponds to locations where the hydride content is the highest, where hydrides are the most radial and continuous, or where the hoop stress is expected to be the highest. In addition, the RHCP and the RHCP^{45} are still limited in their ability to predict high-temperature fracture behavior based on a low-temperature microstructure. Contrarily to previous metrics, this limitation can be minimized by using high-temperature fracture toughness coefficients, but cannot be fully overcome. As discussed in Section 5, at higher temperatures, hydride dissolution can lead to significant microstructure changes, and RHCP values for the low-temperature microstructure might not remain relevant as more plastic deformation occurs in the zirconium matrix. Finally, all the metrics discussed here to quantify hydride morphology fall short when they attempt to correlate exactly with crack propagation. Crack propagation is a 3D phenomenon, and it cannot be fully captured by metrics based on 2D microstructures. This shortcoming is not necessarily due to the definitions of the metrics, as extending them to a 3D domain is possible. For the RHCP, finding a linear path or a surface across a 3D microstructure is feasible. Rather, it remains challenging today to obtain an accurate description of the hydride microstructure and crack propagation path in three dimensions. Overcoming this limitation could lead to significant advances in quantifying hydride morphology and linking it to hydrogen embrittlement.

While working on this study, the authors found that only a few papers made available the micrographs used in their studies. This lack of available data prevented the current study to perform a more comprehensive analysis of the microstructures of the most influential works on the link between hydride microstructures and hydrogen embrittlement. To help address this issue, the authors recommend that in future experimental studies, the micrographs are made available for new studies to be able to link fracture analysis to microstructure.

7. Conclusion

Properly characterizing hydride microstructure is key to studying hydride induced embrittlement of Zr alloy components. This work presents a new metric, the RHCP, to quantify hydride microstructure and relate it to crack propagation. This new metric is designed to bridge the structure, properties, and performance of hydrided zirconium. The RHCP uses a genetic algorithm to find a path through the microstructure by connecting hydrides. The RHCP overcomes some of the limitations of the existing metrics to better discriminate between microstructures and provide a characterization that relates closely to the mechanisms of crack propagation. This metric is given two variations: a definition that minimizes the path length (RHCP), and a definition that respects a 45° angle

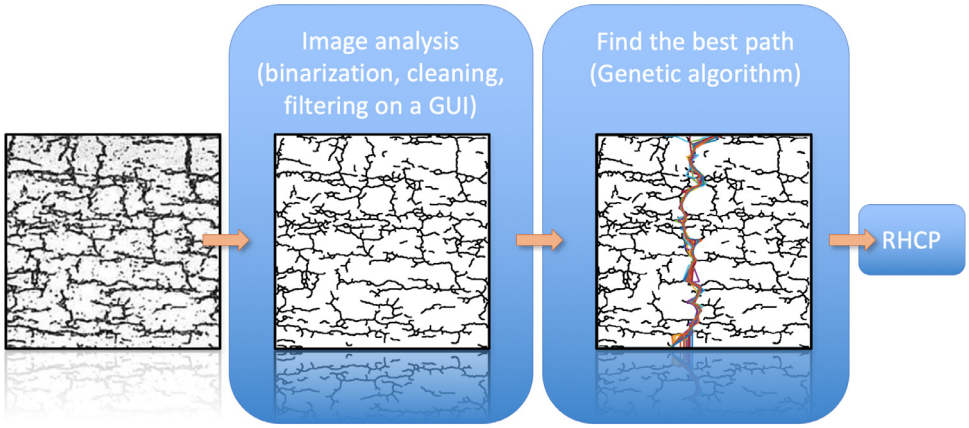

Fig. A.1. Diagrams of the structure of the MATLAB code for the RHCP/RHCP^{45} algorithms. Every MATLAB code include a GUI to binarize the micrographs, and then derives the measured value of the metric. A link to the MATLAB codes is available in Section 8.

in the zirconium phase (RHCP^{45}). The RHCP is more stable with respect to changes in microstructure and the RHCP^{45} better captures crack propagation mechanisms. Existing metrics (RHF, HCC, RHCF), the RHCP, and the RHCP^{45} have been implemented in MATLAB, verified, and validated. In particular, this study shows that the MATLAB implementations of the new definitions offer reliable and consistent results, depend less on the user than manual measurements, and consume less time. When validated against experimental results, RHCP^{45} was shown to correlate better with low temperature fracture behavior than existing metrics. Furthermore, the RHCP^{45} reasonably predicts crack morphology based on the hydride micrograph. While currently applied to zirconium hydride microstructures, the metrics introduced in this study can easily be adapted to quantify the morphology of other two-phase systems.

8. Data Availability

The MATLAB code for the RHF, the HCC, the RHCF, the RHCP, and the RHCP$^{\theta_0}$ as well as the validation and verification micrographs are available at: https://github.com/simopier/QuantifyingHydrideMicrostructure.

Declaration of Competing Interest

The authors declare that they have no known competing financial interests or personal relationships that could have appeared to influence the work reported in this paper.

CRediT authorship contribution statement

Pierre-Clément A. Simon: Conceptualization, Methodology, Software, Validation, Visualization, Writing - original draft, Writing - review & editing. **Cailon Frank:** Software, Validation, Visualization, Writing - review & editing. **Long-Qing Chen:** Supervision, Conceptualization, Validation, Writing - review & editing. **Mark R. Daymond:** Supervision, Conceptualization, Validation, Writing - review & editing. **Michael R. Tonks:** Supervision, Conceptualization, Validation, Writing - review & editing. **Arthur T. Motta:** Supervision, Conceptualization, Validation, Writing - review & editing, Funding acquisition.

Acknowledgements

This work was performed with the support of the DOE NEUP IRP-17-13708 project “Development of a Mechanistic Hydride Behavior Model for Spent Fuel Cladding Storage and Transportation”.

The authors thank Floyd Hilty from the University of Florida for sharing his genetic algorithm and for his assistance in adapting the algorithm to this project.

The validation of the algorithms was made possible by the help of Florian Passelaigue, Jonathan Balog, Joshua May, Matthew Durbin, Pierre Bouhaddane, and Soyoung Kang from The Pennsylvania State University, Floyd Hilty and Shuaifang Zhang from the University of Florida, and Igor Cherubin and Fei Long from Queen’s University, who volunteered to measure the RHF and the RHCP using the different methods to validate the new definitions and implementations.

The authors also thank Ju-Seong Kim from the Korea Atomic Energy Research Institute for sharing the high-resolution microstructures published in [50].

Appendix A. Presentation of the MATLAB Code

The MATLAB codes developed for this study are presented here and illustrated in Fig. A.1. Given a microstructure, MATLAB codes guide the user through the binarization process by using a Graphical User Interface (GUI). It identifies which parts of the micrographs correspond to hydrides. In particular, it can homogenize lighting on the micrographs and filter out impurities. Once the user is satisfied with the binary image, the MATLAB code performs the analysis corresponding to the metrics. In the case of the RHCP or the RHCP^{45}, the code then divides the image into several bands (see Section 3.2) and uses a genetic algorithm to find the best paths within each band. It then merges these paths to create a new generation for the genetic algorithm. The best global path provides the RHCP value of the micrograph. Both codes can analyze micrographs in batch, and save all measurements. Every code and more information are available at the link provided in Section 8.

References

[1] A.T. Motta, L. Capolungo, L.-Q. Chen, M.N. Cinbiz, M.R. Daymond, D.A. Koss, E. Lacroix, G. Pastore, P.-C.A. Simon, M.R. Tonks, B.D. Wirth, M.A. Zikry, Hydrogen in zirconium alloys: a review, J. Nucl. Mater. 518 (2019) 440–460, doi:10.1016/J.JNUCMAT.2019.02.042. https://www.sciencedirect.com/science/article/pii/S0022311518316763

[2] K.B. Colas, A.T. Motta, M.R. Daymond, J.D. Almer, Effect of thermo-mechanical cycling on zirconium hydride reorientation studied in situ with synchrotron X-ray diffraction, J. Nucl. Mater. 440 (2013) 586–595, doi:10.1016/j.jnucmat.2013.04.047. http://www.sciencedirect.com/science/article/pii/S0022311513006557

[3] E. Lacroix, A.T. Motta, J.D. Almer, Experimental determination of zirconium hydride precipitation and dissolution in zirconium alloy, J. Nucl. Mater. 509

(2018) 162–167, doi:10.1016/j.jnucmat.2018.06.038. https://www.sciencedirect.com/science/article/pii/S0022311517317798
[4] J.J. Kearns, Terminal solubility and partitioning of hydrogen in the alpha phase of zirconium, Zircaloy-2 and Zircaloy-4, J. Nucl. Mater. 22 (3) (1967) 292–303, doi:10.1016/0022-3115(67)90047-5. http://www.scopus.com/inward/record.url?eid=2-s2.0-8844286736&partnerID=tZOtx3y1
[5] C.E. Ells, Hydride precipitates in zirconium alloys: a review, J. Nucl. Mater. 28 (2) (1968) 129–151, doi:10.1016/0022-3115(68)90021-4.
[6] K.B. Colas, A.T. Motta, J.D. Almer, M.R. Daymond, M. Kerr, A.D. Banchik, P. Vizcaino, J.R. Santisteban, In situ study of hydride precipitation kinetics and re-orientation in Zircaloy using synchrotron radiation, Acta Materialia 58 (20) (2010) 6575–6583, doi:10.1016/j.actamat.2010.07.018. http://www.sciencedirect.com/science/article/pii/S1359645410004520
[7] K. Colas, A. Motta, M.R. Daymond, J. Almer, Mechanisms of hydride reorientation in Zircaloy-4 studied in situ, in: Zirconium in the Nuclear Industry: 17th Volume, volume STP 1543„ 2015, pp. 1107–1137, doi:10.1520/STP154320120168.
[8] L.G. Bell, R.G. Duncan, Hydride Orientation in Zr-2.5%Nb; How it is Affected by Stress, Temperature and Heat Treatment, Report AECL-5110, 1975. https://inis.iaea.org/search/search.aspx?orig_q=RN:6217504
[9] M.C. Billone, T.A. Burtseva, R.E. Einziger, Ductile-to-brittle transition temperature for high-burnup cladding alloys exposed to simulated drying-storage conditions, J. Nucl. Mater. 433 (1-3) (2013) 431–448, doi:10.1016/j.jnucmat.2012.10.002. http://www.sciencedirect.com/science/article/pii/S0022311512005181
[10] M.N. Cinbiz, D.A. Koss, A.T. Motta, The influence of stress state on the reorientation of hydrides in a zirconium alloy, J. Nucl. Mater. 477 (2016) 157–164, doi:10.1016/j.jnucmat.2016.05.013. http://www.sciencedirect.com/science/article/pii/S0022311516301957
[11] G. Gajowiec, M. Bartmański, B. Majkowska-Marzec, A. Zieliński, B. Chmiela, M. Derezulko, et al., Hydrogen embrittlement and oxide layer effect in the cathodically charged Zircaloy-2, Materials 13 (8) (2020) 1913, doi:10.3390/ma13081913.
[12] A.C. Wallace, G.K. Shek, O.E. Lepik, Effects of hydride morphology on Zr-2.5Nb fracture toughness, Zirconium in the Nuclear Industry: Eighth International Symposium, ASTM International, 100 Barr Harbor Drive, PO Box C700, West Conshohocken, PA 19428-2959, 2008, pp. 66–88, doi:10.1520/STP18858S. http://www.astm.org/doiLink.cgi?STP18858S, STP*1023-EB*.
[13] H.H. Hsu, L.W. Tsay, Effect of hydride orientation on fracture toughness of Zircaloy-4 cladding, J. Nucl. Mater. 408 (1) (2011) 67–72, doi:10.1016/j.jnucmat.2010.10.068.
[14] H.H. Hsu, M.F. Chiang, Y.C. Chen, The influence of hydride on fracture toughness of recrystallized Zircaloy-4 cladding, J. Nucl. Mater. 447 (1-3) (2014) 56–62, doi:10.1016/j.jnucmat.2013.12.028. http://www.sciencedirect.com/science/article/pii/S0022311513013226
[15] P.A. Raynaud, D.A. Koss, A.T. Motta, Crack growth in the through-thickness direction of hydrided thin-wall Zircaloy sheet, J. Nucl. Mater. 420 (1-3) (2012) 69–82, doi:10.1016/j.jnucmat.2011.09.005. http://www.sciencedirect.com/science/article/pii/S0022311511008385
[16] A. Racine, Influence de l'orientation des hydrures sur les modes de déformation, d'endommagement et de rupture du Zircaloy-4 hydruré, Ecole Polytechnique, 2005 Ph.D. thesis. http://pastel.archives-ouvertes.fr/pastel-00002307%5Cnhttp://files/85/pastel-00002307.html
[17] A. Racine, M. Bornert, C. Sainte-Catherine, C. Cappelaere, D. Caldemaison, Experimental investigation of strain, damage and failure of hydrided zirconium alloys with various hydride orientations, in: 11th International Conference on Fracture 2005, ICF11, volume 5, 2005, pp. 3377–3382.
[18] M.D. Callaghan, W.Y. Yeung, M.I. Ripley, D.G. Carr, Measurement of fracture toughness of hydrided Zircaloy - 4, Materials Forum volume 27 (2004) 68–73. http://citeseerx.ist.psu.edu/viewdoc/summary?doi=10.1.1.426.5256
[19] G. Bertolino, G. Meyer, J. Perez Ipiña, Effects of hydrogen content and temperature on fracture toughness of Zircaloy-4, J. Nucl. Mater. 320 (3) (2003) 272–279, doi:10.1016/S0022-3115(03)00193-4.
[20] G. Bertolino, G. Meyer, J. Perez Ipiña, In situ crack growth observation and fracture toughness measurement of hydrogen charged Zircaloy-4, J. Nucl. Mater. 322 (1) (2003) 57–65, doi:10.1016/S0022-3115(03)00305-2.
[21] G. Bertolino, J. Perez Ipiña, G. Meyer, Influence of the crack-tip hydride concentration on the fracture toughness of Zircaloy-4, J. Nucl. Mater. 348 (1-2) (2006) 205–212, doi:10.1016/j.jnucmat.2005.09.017.
[22] J.S. Dubey, S.L. Wadekar, R.N. Singh, T.K. Sinha, J.K. Chakravartty, et al., Assessment of hydrogen embrittlement of Zircaloy-2 pressure tubes using unloading compliance and load normalization techniques for determining J-R curves, J. Nucl. Mater. 264 (1-2) (1999) 20–28, doi:10.1016/S0022-3115(98)00487-5.
[23] S.-i. Honda, Fracture toughness of Zr-2.5 wt% Nb pressure tubes, Nucl. Eng. Des. 81 (2) (1984) 159–167, doi:10.1016/0029-5493(84)90003-7.
[24] H.H. Hsu, An evaluation of hydrided Zircaloy-4 cladding fracture behavior by X-specimen test, J. Alloys Compd. 426 (1–2) (2006) 256–262, doi:10.1016/j.jallcom.2005.12.113.
[25] G.D. Fearnehough, A. Cowan, The effect of hydrogen and strain rate on the "ductile-brittle" behaviour of Zircaloy, J. Nucl. Mater. 22 (2) (1967) 137–147, doi:10.1016/0022-3115(67)90023-2.
[26] P.H. Davies, C.P. Stearns, Fracture toughness testing of Zircaloy-2 pressure tube material with radial hydrides using direct-current potential drop, in: ASTM Special Technical Publication, ASTM, 1986, pp. 379–400, doi:10.1520/stp17408s. http://www.astm.org/DIGITAL_LIBRARY/STP/PAGES/STP17408S.htm
[27] J. Desquines, D. Drouan, M. Billone, M.P. Puls, P. March, S. Fourgeaud, C. Getrey, V. Elbaz, M. Philippe, Influence of temperature and hydrogen content on stress-induced radial hydride precipitation in Zircaloy-4 cladding, J. Nucl. Mater. 453 (1-3) (2014) 131–150, doi:10.1016/j.jnucmat.2014.06.049.
[28] J. Desquines, D. Drouan, S. Guilbert, P. Lacote, Embrittlement of pre-hydrided Zircaloy-4 by steam oxidation under simulated LOCA transients, J. Nucl. Mater. 469 (2016) 20–31, doi:10.1016/j.jnucmat.2015.11.008.
[29] D. Hardie, M.W. Shanahan, Stress reorientation of hydrides in zirconium-2.5% niobium, J. Nucl. Mater. 55 (1) (1975) 1–13, doi:10.1016/0022-3115(75)90132-4.
[30] K.N. Jang, K.T. Kim, The effect of neutron irradiation on hydride reorientation and mechanical property degradation of zirconium alloy cladding, Nucl. Eng. Technol. 49 (7) (2017) 1472–1482, doi:10.1016/j.net.2017.05.006. http://www.sciencedirect.com/science/article/pii/S1738573317303327
[31] R.P. Marshall, Influence of fabrication history on stress-oriented hydrides in Zircaloy tubing, J. Nucl. Mater. 24 (1) (1967) 34–48, doi:10.1016/0022-3115(67)90078-5. http://www.sciencedirect.com/science/article/pii/0022311567900785
[32] M.R. Louthan, R.P. Marshall, Control of hydride orientation in Zircaloy, J. Nucl. Mater. 9 (2) (1963) 170–184, doi:10.1016/0022-3115(63)90132-6.
[33] J.B. Bai, N. Ji, D. Gilbon, C. Prioul, D. François, Hydride embrittlement in ZIRCALOY-4 plate: Part II. Interaction between the tensile stress and the hydride morphology, Metallurgical and Materials Transactions A 25 (6) (1994) 1199–1208, doi:10.1007/BF02652294. https://link.springer.com/article/10.1007/BF02652294
[34] H.C. Chu, S.K. Wu, R.C. Kuo, Hydride reorientation in Zircaloy-4 cladding, J. Nucl. Mater. 373 (1-3) (2008) 319–327, doi:10.1016/j.jnucmat.2007.06.012. http://www.sciencedirect.com/science/article/pii/S0022311507008380?via%3Dihub
[35] A.M. Alam, C. Hellwig, Cladding tube deformation test for stress reorientation of hydrides, in: ASTM Special Technical Publication, volume 1505 STP, American Society for Testing and Materials, 2009, pp. 635–650, doi:10.1520/stp48160s. http://www.astm.org/DIGITAL_LIBRARY/STP/PAGES/STP48160S.htm
[36] S. Valance, J. Bertsch, Hydrides reorientation investigation of high burn-up PWR fuel cladding, J. Nucl. Mater. 464 (2015) 371–381, doi:10.1016/j.jnucmat.2015.05.003.
[37] H.J. Cha, J.J. Won, K.N. Jang, J.H. An, K.T. Kim, Tensile hoop stress-, hydrogen content- and cooling rate-dependent hydride reorientation behaviors of Zr alloy cladding tubes, J. Nucl. Mater. 464 (2015) 53–60, doi:10.1016/j.jnucmat.2015.04.027.
[38] R.K. Sharma, A.K. Bind, G. Avinash, R.N. Singh, A. Tewari, B.P. Kashyap, Effect of radial hydride fraction on fracture toughness of CWSR Zr-2.5%Nb pressure tube material between ambient and 300 °C temperatures, J. Nucl. Mater. 508 (2018) 546–555, doi:10.1016/J.JNUCMAT.2018.06.003. https://www.sciencedirect.com/science/article/pii/S002231151830120X
[39] S. Sunil, A. Gopalan, A.K. Bind, R.K. Sharma, T.N. Murty, R.N. Singh, Effect of radial hydride on delayed hydride cracking behaviour of Zr-2.5Nb pressure tube material, J. Nucl. Mater. 542 (2020) 152457, doi:10.1016/j.jnucmat.2020.152457.
[40] O.N. Pierron, Influence of hydride blisters on failure of Zircaloy-4 sheet, The Pennsylvania State University, 2002 M.S. in Materials Science.
[41] O.N. Pierron, D.A. Koss, A.T. Motta, K.S. Chan, The influence of hydride blisters on the fracture of Zircaloy-4, J. Nucl. Mater. 322 (1) (2003) 21–35, doi:10.1016/S0022-3115(03)00299-X. http://www.sciencedirect.com/science/article/pii/S002231150300299X
[42] T.J. Walker, Characterization of the fracture toughness of Zircaloy, Nucl. Technol. 16 (1972) 509–520, doi:10.13182/NT72-A31219.
[43] A. Machiels, Fracture Toughness Data for Zirconium Alloys Application to Spent Fuel Cladding in Dry Storage EPRI Project Manager, Technical Report, EPRI, Palo Alto, CA, 2001 1001281.
[44] L.A. Simpson, C.D. Cann, Fracture toughness of zirconium hydride and its influence on the crack resistance of zirconium alloys, J. Nucl. Mater. 87 (2-3) (1979) 303–316, doi:10.1016/0022-3115(79)90567-1. https://www.sciencedirect.com/science/article/pii/0022311579905671
[45] V. Grigoriev, B. Josefsson, B. Rosborg, Fracture toughness of Zircaloy cladding tubes, ASTM Special Technical Publication 1295 (1996) 431–447, doi:10.1520/stp16184s. http://www.astm.org/DIGITAL_LIBRARY/STP/PAGES/STP16184S.htm
[46] F.W. Hilty, M.R. Tonks, Development and application of a microstructure dependent thermal resistor model for UO2 reactor fuel with high thermal conductivity additives, J. Nucl. Mater. 540 (2020) 152334, doi:10.1016/j.jnucmat.2020.152334. https://linkinghub.elsevier.com/retrieve/pii/S0022311520303561
[47] K.B. Colas, Fundamental experiments on hydride reorientation in Zircaloy, The Pennsylvania State University, 2012 Ph.D. thesis in Nuclear Engineering. http://adsabs.harvard.edu/abs/2012PhDT.....309C
[48] M. Nedim Cinbiz, M. Balooch, X. Hu, A. Amroussia, K. Terrani, Nanoindentation study of bulk zirconium hydrides at elevated temperatures, Journal of Alloysand Compounds 726 (2017) 41–48, doi:10.1016/j.jallcom.2017.07.319. http://www.sciencedirect.com/science/article/pii/S0925838817327044
[49] H.C. Chu, S.K. Wu, K.F. Chien, R.C. Kuo, Effect of radial hydrides on the axial and hoop mechanical properties of Zircaloy-4 cladding, J. Nucl. Mater. 362 (1) (2007) 93–103, doi:10.1016/j.jnucmat.2006.11.008.
[50] J.S. Kim, T.H. Kim, D.H. Kook, Y.S. Kim, et al., Effects of hydride morphology on the embrittlement of Zircaloy-4 cladding, J. Nucl. Mater. 456 (2015) 235–245, doi:10.1016/j.jnucmat.2014.09.025.
[51] R.S. Daum, S. Majumdar, Y. Liu, M.C. Billone, Radial-hydride embrittlement of high-burnup Zircaloy-4 fuel cladding, J. Nucl. Sci. Technol. 43 (9) (2006) 1054–1067, doi:10.1080/18811248.2006.9711195. http://www.tandfonline.com/doi/abs/10.1080/18811248.2006.9711195